PROCEEDINGS OF SCIENCE

Recent progresses in few-nucleon structure and dynamics within chiral effective field theory

Laura Elisa Marcucci,[a,b,*] **Alex Gnech**[c,d] **and Michele Viviani**[b]

[a] *Department of Physics, University of Pisa, Largo B. Pontecorvo 3, Pisa, Italy*
[b] *Istituto Nazionale di Fisica Nucleare, Sezione di Pisa, Largo B. Pontecorvo 3, Pisa, Italy*
[c] *Department of Physics, Old Dominion University, Norfolk, VA 23529*
[d] *Theory Center, Jefferson Lab, Newport News, VA 23610*
E-mail: laura.elisa.marcucci@unipi.it, agnech@odu.edu, michele.viviani@pi.infn.it

The most recent progresses made within the framework of chiral effective field theory for few-nucleon structure and low-energy reactions are here presented. In particular, for the $A = 2$ sector, the study of muon capture on deuteron is reviewed. Then, the results obtained using the Hyperspherical Harmonics *ab-initio* method for the ^{4}He monopole form factor and the $^3\mathrm{He}(\vec{n}, p)^3\mathrm{H}$ parity-conserving asymmetry are described.

The 11th International Workshop on Chiral Dynamics (CD2024)
26-30 August 2024
Ruhr University Bochum, Germany

*Speaker

 ISSN 1824-8039 . Published by SISSA Medialab.

PoS(CD2024)103

1. Introduction

Recent advances in the understanding of few-nucleon systems have been significantly influenced by the development and application of chiral effective field theory (ChEFT). This theoretical framework provides a systematic approach to describe nuclear forces and currents, grounded in the symmetries of quantum chromodynamics (QCD). The work presented here summarizes the recent progresses made in studies of few-nucleon reactions, using various ChEFT potentials and related electro-weak currents, and employing, for systems with $A > 2$, the Hyperspherical Harmonics (HH) *ab-initio* method to achieve precise calculations.

This contribution is organized in the following sections: in Sec. 2 we briefly review the theoretical formalism adopted for the present studies, focusing on the electro-weak nuclear current obtained within ChEFT, and on the HH *ab-initio* method; in Sec. 3 we present some selected results for the $A = 2$ and $A = 4$ systems, in particular for the muon capture on deuteron, the monopole form factor of ^{4}He, and the parity-conserving asymmetry in the $^3\mathrm{He}(\vec{n}, p)^3\mathrm{H}$ reaction. We conclude in Sec. 4 with a summary and an outlook.

2. Theoretical formalism

As mentioned above, ChEFT is the adopted theoretical framework, both for nuclear interactions and currents. The description of ChEFT nuclear interactions is clearly beyond the scope of this contribution. We only summarize the models adopted in the studies reviewed here. For a recent review see Ref. [1]. For the nucleon-nucleon (NN) interaction, we have focused on the next-to-next-to-next-to leading order (N3LO) potentials of Ref. [2, 3] (EM), with cutoff values of $\Lambda = 500, 600$ MeV, and on the more recent potentials of Ref. [4] (EMN), derived from LO up to N4LO, with cutoff values $\Lambda = 450, 500, 550$ MeV. All these potentials are non local. Additionally, we have considered also the so-called Norfolk potentials of Ref. [5–7] (NV). These are local N3LO interactions, which retain additionally Δ-isobar degrees of freedom. The four NV models considered here differ for the range of laboratory energy employed in the fitting procedure (class I or II), and for the values of the short- and long-range cutoffs (model a or b).

The three-nucleon (3N) interaction needed to describe the $A = 4$ bound and scattering systems, is constructed consistently with the NN potentials. In particular, we have included the 3N interaction at N2LO, the first chiral order at which 3N interactions appear, with a cutoff function chosen to make this interaction local. The low-energy constants (LECs) c_D and c_E which enter in the 3N interaction have been obtained in all the cases by reproducing the triton binding energy and the Gamow-Teller matrix element of tritium β-decay (see below for more details). Their values can be found in Refs. [7–9] for the EM, EMN and NV potentials, respectively.

In the study of the muon capture and the ^{4}He monopole form factor, the electro-weak nuclear current and charge operators are crucial components of the calculation. However, in the case of the ^{4}He monopole form factor, the main contribution arises from the LO (one-body) charge operator. Therefore, in this section we will focus on the weak operators. Note that the vector weak operators are related to their electromagnetic counterpart via a rotation in the isospin space. Two prominent research groups, the Bochum and JLab-Pisa collaborations, have developed different power counting schemes for the weak operators, leading also to different expressions. Due to lack

Oper.	LO (Q^{-3})	NLO (Q^{-2})	N2LO (Q^{-1})	N3LO (Q^{0})
$\rho(A)$	–	1b(NR)	OPE	–
$\mathbf{j}(A)$	1b(NR)	–	1b(RC) OPE-Δ^*	CT(d_R) OPE
$\rho(V)$	1b(NR)	–	1b(RC)	OPE(RC)
$\mathbf{j}(V)$	–	1b(NR)	OPE	1b(RC) OPE-Δ^*

Table 1: Ordering of the chiral electro-weak currents as organized by the JLab-Pisa group. The acronyms are defined in the text. The star is used for those terms that do not appear for the EM and EMN interactions (Δ-less potentials).

of space, we focus here on the work of the JLab-Pisa group, and the various contributions, together with the corresponding chiral orders, are summarized in Table 1. As it can be seen from the table, indicating with Q the low-energy momentum scale of the theory, the non-relativistic (NR) one-body (1b) contributions appear at order Q^{-3} (LO) for the axial current ($\mathbf{j}(A)$) and vector charge ($\rho(V)$) operators, and at order Q^{-2} (NLO) for the axial charge ($\rho(A)$) and vector current ($\mathbf{j}(V)$) operators. At NLO, there are no contributions to $\mathbf{j}(A)$ and $\rho(V)$. At order Q^{-1} (N2LO), the one-pion exchange (OPE) contributions appear in $\rho(A)$ and $\mathbf{j}(V)$, while in $\rho(V)$ and $\mathbf{j}(A)$ we have contributions from relativistic corrections (RC) to the 1b term. In the axial current $\mathbf{j}(A)$, also the one-pion-exchange contribution with an intermediate Δ-isobar excitation (OPE-Δ) should be retained at N2LO, when the Δ-isobar is considered as an explicit degree of freedom, as in the case of the NV potentials. At order Q^0 (N3LO), there are no contributions to $\rho(A)$, while $\rho(V)$ presents the OPE contribution. The vector current $\mathbf{j}(V)$ retains at this order RC to the 1b term and possibly OPE-Δ for the NV potentials. Finally, at N3LO, the first contact term (CT) appears in $\mathbf{j}(A)$, together with OPE. At this order, therefore, the LEC d_R has to be fitted. This LEC is related to the LEC c_D entering the 3N interaction, and therefore a quite common procedure for determining c_D, together with the LEC c_E in the 3N interaction, is to fit to the triton binding energy and the Gamow-Teller in tritium β-decay [7–9]. At order Q^1 (N4LO) there are additional contributions to all the operators. However, these contributions are not yet complete for the EMN and NV interactions used in the present studies, and therefore we do not discuss them here. Finally, we remark that in the study of the muon capture on deuteron of Ref. [9], also the different power counting scheme of the Bochum group has been considered (see Table III of Ref. [9]). However, here we narrow our discussion to the results obtained with the operators derived by the JLab-Pisa group [7, 10, 11].

A crucial ingredient for the study of the $A = 4$ processes, is the development of an accurate *ab-initio* method to solve the $A = 4$ bound and scattering problems. In this work, we used the HH method, which is nowadays among the most accurate methods for both bound and scattering few-nucleon systems. In particular, using the Rayleigh-Ritz and the Kohn variational principles for bound states and scattering states, respectively, the HH method has been applied to the $A = 3, 4, 6$ nuclei [12–15], and the $A = 3, 4$ scattering states [13, 17]. In this contribution, we focus on the HH method at work for the $A = 4$ scattering states [17]. We consider a specific clusterization $A + B$, denoted by the index γ, with $\gamma = 1$ (2) referring to the $p + {}^3\mathrm{H}$ ($n + {}^3\mathrm{He}$). The wave function

$\Psi^{\gamma LS}$ describing incoming clusters with relative orbital angular momentum L and channel spin S, coupled to the total angular momentum JJ_z, can be written as the sum of a core part, $\Psi_C^{\gamma LS}$, and an asymptotic part, $\Psi_A^{\gamma LS}$. The core part $\Psi_C^{\gamma LS}$ describes the four particles when they are close to each other. It is expanded on the spin-isospin-HH functions, encoding all the spin-isospin structure of the wave function for a given J^π state, π being the parity, multiplied by known functions of the hyper-radius ρ, typically Laguerre polynomials (see Ref. [16] for more details). The expansion coefficients are clearly unknown and need to be determined. The asymptotic part $\Psi_A^{\gamma LS}$ describes the relative motion of the two clusters in the asymptotic regions, where the mutual interaction is negligible (except for the long-range Coulomb interaction). It can be decomposed as a linear combination of the functions $\Omega_{\gamma LS}^{F/G}$ defined as

$$\Omega^F_{\gamma LS} = \frac{1}{\sqrt{4}}\mathcal{A}\left\{\left[Y_L(\hat{y}_\gamma)[\Phi_\gamma(ijk)s_l]_S\right]_{JJ_z}\frac{F_L(\eta_\gamma, q_\gamma y_\gamma)}{q_\gamma y_\gamma}\right\}, \tag{1}$$

$$\Omega^G_{\gamma LS} = \frac{1}{\sqrt{4}}\mathcal{A}\left\{\left[Y_L(\hat{y}_\gamma)[\Phi_\gamma(ijk)s_l]_S\right]_{JJ_z}\frac{G_L(\eta_\gamma, q_\gamma y_\gamma)}{q_\gamma y_\gamma}(1-e^{-\beta y_\gamma})^{2L+1}\right\}, \tag{2}$$

where y_γ is the distance between the center-of-mass of clusters A and B, q_γ is the magnitude of the relative momentum between the two clusters, $\Phi_{\gamma=1,2}(ijk) \equiv \Phi_{^3\mathrm{H},^3\mathrm{He}}(ijk)$ are the $A = 3$ bound state wave functions, obtained also within the HH method, and the symbols $\mathcal{A}$ indicate that the expressions between the curly brackets have to be properly antisymmetrized. The functions $F_L(\eta_\gamma, q_\gamma y_\gamma)$ and $G_L(\eta_\gamma, q_\gamma y_\gamma)$ describe the asymptotic radial motion of clusters A and B, and are the regular and irregular Coulomb functions, respectively, with η_γ being the Sommerfeld parameter, proportional to the clusters charges. If one of the clusters is a neutron, as in the $n - {}^3$He scattering, then $\eta_{\gamma=2} = 0$, and the functions F_L and G_L reduce to the regular and irregular spherical Bessel functions. Finally, the term $(1 - e^{-\beta y_\gamma})^{2L+1}$ in Eq. (2) is used to "regularize" the irregular Coulomb function for $y_\gamma \to 0$, with the parameter β usually chosen to be $\beta = 0.25$ fm^{-1}.

Instead of working with $\Omega_{\gamma LS}^{F,G}$, it is convenient to define

$$\Omega^\pm_{\gamma LS} = \Omega^G_{\gamma LS} \pm \mathrm{i}\Omega^F_{\gamma LS}\,, \tag{3}$$

where $\Omega^+_{\gamma LS}$ ($\Omega^-_{\gamma LS}$) describes the outgoing (ingoing) relative motion of the clusters specified by γ. In this way, $\Psi_A^{\gamma LS}$ can be rewritten as

$$\Psi_A^{\gamma,L,S} = \Omega^F_{\gamma,L,S} + \sum_{\gamma',L',S'} \mathcal{T}^{\gamma,\gamma'}_{L,S;L',S'}\Omega^+_{\gamma',L',S'}\,, \tag{4}$$

where the sum over L' and S' is over all values compatible with the given J and parity π, and the parameters $\mathcal{T}^{\gamma,\gamma'}_{LS,L'S'}$ are the so-called T-matrix elements, obtained, together with the expansion coefficients of the core part, using the Kohn variational principle. For more details see Ref. [17].

3. Results

We present some selected results obtained within the theoretical framework highlighted in Sec. 2. In particular, in Subsec. 3.1 we summarize the results of Ref. [9] for the muon capture on deuteron, in Subsec. 3.2 those of Ref. [16] for the ^{4}He monopole form factor, and in Subsec. 3.3 those of Ref. [18] for the parity-conserving asymmetry in the $^3\mathrm{He}(\vec{n}, p)^3\mathrm{H}$ reaction.

3.1 Muon capture on deuteron

Muon capture on deuteron, i.e. the reaction $\mu^- + d \to n + n + \nu_\mu$, can happen in the initial doublet or quartet hyperfine state. In Ref. [9], the capture rates in both states have been studied, but here we focus only on the largest one, i.e. on the capture rate in the initial doublet state, $\Gamma^{1/2}$. A large variety of ChEFT potential models have been implemented. These are the EMN models, with cutoff $\Lambda = 450, 500, 550$ MeV, from LO up to N3LO, and the NV potentials NVIa, NVIb, NVIIa, NVIIb. The reason behind the choice of these models resides in the novelty of this work: in fact, several studies of muon capture on deuteron also in ChEFT have been performed, but only in Ref. [9], the calculated values of $\Gamma^{1/2}$ are accompanied by a robust theoretical uncertainty evaluation. The sources of uncertainties are: (i) the LECs in the nuclear axial current, and in particular the LEC d_R, and the axial radius r_A entering the definition of the axial form factor $g_A(q^2)$ through the relation $g_A(q^2) = g_A \left(1 - \frac{1}{6} r_A^2 q^2\right)$. For the axial radius, we have adopted $r_A^2 = 0.46(16)$ fm^2 [19]. Since the momentum transfer q for muon capture on deuteron is quite large, the uncertainty on r_A^2 makes a significant impact on the capture rate. At the same time, it is important to study the impact of the uncertainty on the LEC d_R. Such uncertainty is given in Refs. [7, 9] for the NV and EMN interactions. The errors on r_A^2 and d_R have been propagated with standard error propagation techniques, and the theoretical uncertainty on the LECs $\sigma^2_{\rm LECs}$ has been defined as

$$\sigma^2_{\rm LECs} = \left(\frac{\partial \Gamma}{\partial r_A^2}\right)^2 \sigma^2(r_A^2) + \left(\frac{\partial \Gamma}{\partial d_R}\right)^2 \sigma^2(d_R) \ . \tag{5}$$

(ii) A second source of uncertainty is that arising from the truncation of the chiral order both for interactions (I) and currents (C). Starting from Ref. [20], a Bayesian analysis has been performed in order to quantify the standard deviation of the truncation error both for the current and interaction at different orders of the chiral expansion k, $\sigma_k^{C/I}$. In particular, for the current, we have stopped at chiral order $k = 3$ (see Table 1), while for the interaction $k = 4$ (the EMN interactions are derived up to N4LO). However, being the NV potential at fixed N3LO chiral order, σ_k^I cannot be calculated. (iii) A final source of uncertainty is that due to the dependence on various nuclear interaction models. The use of a large number of interaction models, of quite different families, as the EMN and NV potentials, has allowed us to estimate also this uncertainty.

The results for $\Gamma^{1/2}$, $\sigma^C_{k=3}$, $\sigma^I_{k=4}$, and $\sigma_{\rm LECs}$ are given in Table 2, with all uncertainties reported at 68% confidence level (CL). The *nn* final state includes contributions up to total angular momentum $J = 4$. Contributions for larger values of J have been found negligible. Since the N4LO currents are not fully determined, the analysis is performed considering the currents only up to N3LO using the values of d_R fitted consistently at N3LO as well. As it can be seen from inspection of the table, the power counting of the currents has a larger impact on the determination of the truncation errors. This is even more evident with the Bochum group power counting, as reported in Ref. [9]. Although not reported in the table, this power counting gives rise to values for $\sigma^C_{k=3}$ of $\sim 5\ {\rm s}^{-1}$ ($\sim 6\ {\rm s}^{-1}$) for the NV (EMN) potentials. Furthermore, even if the results for $\Gamma^{1/2}$ calculated with all the interactions are compatible within errors, the values of capture rates obtained using the local interactions are systematically lower than the ones obtained using the non-local interactions. This is partially due to the different sign of the contact terms in the axial current at N3LO. Note that the truncation errors associated to the interaction and the currents are studied separately. As a matter of fact, this is not

Model	$\Gamma^{1/2}$	$\sigma^{C}_{k=3}$	$\sigma^{I}_{k=4}$	$\sigma_{\rm LECs}$
NVIa	393.5	1.1	n.a.	3.9
NVIb	393.7	1.1	n.a.	3.9
NVIIa	392.5	1.1	n.a.	3.9
NVIIb	392.6	1.1	n.a.	3.9
EMN450	396.0	2.2	0.3	3.9
EMN500	397.3	2.2	0.3	3.9
EMN550	397.0	2.1	0.4	3.9

Table 2: Muon capture rate on deuteron for all the NV and EMN interactions. In particular, $\Gamma^{1/2}$, in s^{-1}, is the computed value using the currents and the interactions at N3LO, $\sigma^{C(I)}_{k=3(4)}$ is the standard deviation of the truncation error, and $\sigma_{\rm LECs}$ is the uncertainties associated with the LECs appearing in the currents, defined in Eq.(5). All the uncertainties are reported at 68% CL. The uncertainty $\sigma^{I}_{k=4}$ cannot be calculated for the NV potentials, being defined at a fixed order. All the results are given in s^{-1}.

completely correct, because of precise relations between the Hamiltonian and the currents such as current conservation. However, such relations are not completely fulfilled order-by-order by the available currents yet. Therefore, our choice to treat σ^{C}_{k} and σ^{I}_{k} separately is the most practical one.

We show in Fig. 1 the recommended differential capture rate, as function of the kinetic neutron energy, with the bands at 68%, 95%, and 99% CL. These results are obtained averaging the differential capture rates obtained with the large variety of N3LO potential models, i.e. the EMN with $\Lambda = 450, 500, 550$ MeV, and the NVIa, NVIb, NVIIa, and NVIIb potentials, as explained in Ref. [9]. To be remarked that the difference among the bands can be appreciated in fact only at the peak of the spectra, an indication of the accuracy of the calculation.

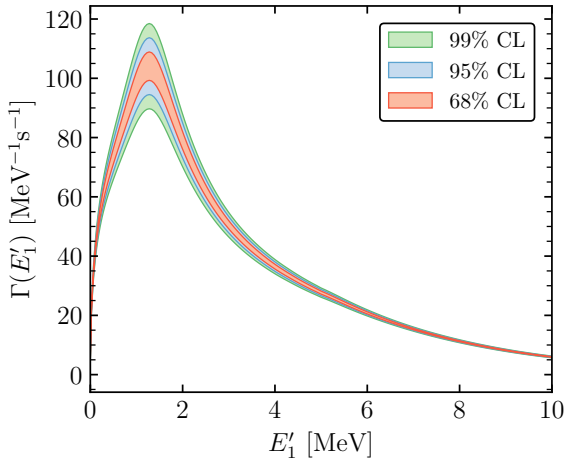

Figure 1: The recommended differential capture rate as function of the kinetic neutron energy E_1'. The green, blue, and red bands represent respectively the 99%, 95%, and 68% CL.

When integrating the differential capture rate of Fig. 1, we obtain the total capture rate, which is found to be $\Gamma_{\rm th} = (395 \pm 6)\,s^{-1}$ at 68% CL. Note that using the Bochum power counting, we obtain $\Gamma_{\rm th} = (395 \pm 10)\,s^{-1}$, still at 68% of CL [9].

3.2 The ^{4}He monopole form factor

The ^{4}He monopole form factor is extracted from the $e + {}^4$He cross section at various energies, and is defined as the ratio between the cross section of the process and the Mott cross section. In the study discussed in this section, we consider energies below the $d + d$ threshold. In this case, the contributions to be included are the $^4\mathrm{He}(e, e'p)^3\mathrm{H}$ and $^4\mathrm{He}(e, e'n)^3\mathrm{He}$ above $n + {}^3$He threshold, and only the $^4\mathrm{He}(e, e'p)^3\mathrm{H}$ below the $n + {}^3$He threshold.

By performing a multipole expansion, and several algebraic steps (see Ref. [16] for all the details), it is possible to demonstrate that the monopole form factor is given by

$$|F_M(q)|^2 = \frac{1}{16\pi} \sum_{\gamma=1,2} \int_0^\infty dE_\gamma \; 8 p_\gamma \mu_\gamma |C_0(q, E_\gamma)|^2 \,, \tag{6}$$

where E_γ is the proton ($\gamma = 1$) or neutron ($\gamma = 2$) energy, μ_γ and p_γ are the 1+3 reduced mass and relative momentum, respectively, and q is the momentum transferred. With $C_0(q, E_\gamma)$ we indicate the reduced matrix element of the Coulomb multipole operator, and it is defined as

$$C_0(q, E_\gamma) = \frac{1}{\sqrt{4\pi}} \langle \Psi^{1+3}_{J=L=S=0} | \hat{\rho}(\boldsymbol{q}) | \Psi(^4\mathrm{He}) \rangle \,, \tag{7}$$

with $\hat{\rho}(\boldsymbol{q})$ being the charge operator.

The result for the form factor $|F_M(q)|$ is shown in Fig. 2. In this calculation, the adopted interactions are the EM N3LO potentials [2], with cutoff $\Lambda = 500$ or 600 MeV, augmented by the 3N N2LO interaction. The calculations are compared with various sets of experimental data [21–24]. The dominant contribution arises from the one-body LO charge operator. In fact, the corrections beyond LO represented by relativistic corrections and meson-exchange currents, are included, but are found to be very small. As it can be seen from the figure, our theoretical predictions are in nice agreement with the MAMI data [24], and the inclusion of terms beyond LO slightly reduces the monopole form factor, especially for large values of q, bringing the calculations very close to the MAMI data. The spread between the calculations obtained with the N3LO500/N2LO500 and N3LO600/N2LO600, reflects our ignorance about the short-range part of the nuclear interaction. Finally, comparing our results with other theoretical calculations, we obtained a nice agreement with Refs. [25–27], but not with Ref. [28]. The origin of this discrepancy is still under investigation.

3.3 The $^3\mathrm{He}(\vec{n}, p)^3\mathrm{H}$ parity-conserving asymmetry

The parity-conserving asymmetry A_{PC} in $^3\mathrm{He}(\vec{n}, p)^3\mathrm{H}$ is defined through the relation

$$\frac{\mathrm{d}\sigma}{\mathrm{d}\Omega} = \left(\frac{\mathrm{d}\sigma}{\mathrm{d}\Omega}\right)_{\mathrm{u}} \left(1 + A_{\mathrm{PV}} \hat{s}_n \cdot \hat{k}_p + A_{\mathrm{PC}} (\hat{s}_n \times \hat{k}_n) \cdot \hat{k}_p\right) \tag{8}$$

where $\frac{\mathrm{d}\sigma}{\mathrm{d}\Omega\,\mathrm{u}}$ is the unpolarized cross section, and $\hat{s}_n$, $\hat{k}_p$, and $\hat{k}_n$ denote unit vectors specifying the directions of the neutron polarization, the outgoing proton momentum, and the incoming neutron beam, respectively. The parity-conserving asymmetry A_{PC} is measured by detecting emitted protons with their momenta in the plane defined by $\hat{s}_n \times \hat{k}_n$ and $\hat{k}_n$, and the parity-violating asymmetry A_{PV} in the plane defined by $\hat{s}_n$ and $\hat{k}_n$. Since the parity-conserving asymmetry A_{PC} is proportional to $1/\lambda_n$, λ_n being the neutron wavelength, the quantity β defined as $\beta = \lambda_n A_{\mathrm{PC}}$ will be considered.

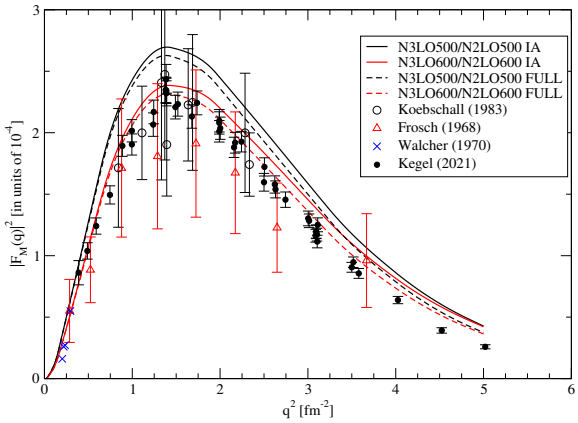

Figure 2: (color online) The monopole form factor $|F_M(q)|^2$, obtained with the EM N3LO potentials, with cutoff $\Lambda = 500$ or 600 MeV, augmented by the 3N N2LO interaction (curves labelled N3LO500/N2LO500 and N3LO600/N2LO600, respectively). The charge operator includes the one-body LO or impulse approximation term (full lines, labelled IA), and terms beyond LO, as described in the text (dashed lines, labelled FULL). The experimental data are from Refs. [21–24].

Interaction	$E_R(0^-)$ [MeV]	$\Gamma(0^-)$ [MeV]	$t^{2,1}_{11,11}$ [fm]	$\beta \times 10^6$ [Å]
N3LO500	0.16	0.41	20.7	− 4.83
N3LO600	0.24	0.51	16.9	− 2.68
NVIa	0.31	0.53	17.3	− 2.61
NVIb	0.30	0.54	13.0	− 0.43
N3LO500/N2LO500	0.06	0.26	30.1	−10.04
N3LO500/N2LO500*	0.14	0.41	18.5	− 2.68
N3LO600/N2LO600	0.09	0.30	25.9	− 5.28
NVIa/3N	0.04	0.36	35.4	−12.17
NVIb/3N	0.12	0.40	23.9	− 5.15
Experimental	0.44	0.84		−1.97 ±0.28 (stat) ±0.12 (sys)

Table 3: Theoretical predictions for the asymmetry β obtained with the HH method and different Hamiltonians: in the first part of the table, only NN interactions are considered, while in the second part also 3N potentials are included. See text for more details. We report in the table also the position $E_R(0^-)$ and width $\Gamma_R(0^-)$ of the ^{4}He $J^\pi = 0^-$ resonance obtained [17], and the values of $t^{2,1}_{11,11}$ as defined in the text.

The calculation of A_{PC} requires to express this observables in terms of the transition matrix elements $\mathcal{T}^{\gamma,\gamma'}_{LS,L'S'}$ defined in Sec. 2. The explicit expression can be found in Ref. [16]. In Table 3 we list the theoretical predictions not only for β, but also the $J^\pi = 0^-$ resonance energy and width, which significantly affect the calculation. Furthermore, we report the value for the matrix element $t^{2,1}_{11,11}$, in the case $J = 0$, defined as $t^{2,1}_{11,11} = \lim_{q_2 \to 0} |\mathcal{T}^{2,1}_{11,11}|/q_2$, q_2 being the relative $n - {}^3$He momentum ($q_{\gamma=2}$). In this way $t^{2,1}_{11,11}$ does not diverge for $q_2 \to 0$, as we know that $\mathcal{T}^{2,1}_{LS,LS} \sim q_2^L$. The matrix element $t^{2,1}_{11,11}$ is in fact the dominant one.

By inspection of the table we can conclude that β is very sensitive to $t^{2,1}_{11,11}$, and that there is a very large model-dependence. In fact, tiny differences in the position of the $J^\pi = 0^-$ resonance result in large changes in $t^{2,1}_{11,11}$. The large model-dependence for β is due to the fact that the various $\mathcal{T}^{\gamma,\gamma'}_{LS,L'S'}$ contributions tend to cancel each other, in particular the largest ones. Furthermore, it should be remarked, as mentioned in Ref. [16], that without $\mathcal{T}^{2,1}_{11,11}$, A_{PC} would be positive, at variance with what is found experimentally. Finally, we should notice that using the N3LO500/N2LO500 or the N3LO500/N2LO500* interaction, which differ only for the values of c_D and c_E in the 3N force, we obtain very different results. Therefore, this observable is very sensitive to the details of the 3N force. The difference between the N3LO500/N2LO500 and N3LO600/N2LO600 results shows the sensitivity of β to the cutoff values, and consequently to the different treatment of the short-range physics. This large model-dependence represents an opportunity, i.e. a possible path to obtain further information on the 3N interaction.

4. Conclusion and outlook

In the present contribution we have presented some recent progresses made within the framework of chiral effective field theory for few-nucleon structure and low-energy reactions. In the $A = 2$ sector, we have summarized the results obtained in Ref. [9] for the rate of muon capture on deuteron. This study is the first one for this process where a Bayesian analysis has allowed to derive the theoretical uncertainty of the prediction in a very robust way. Then, we have focused on the $A = 4$ sector, and we have presented the results obtained using the Hyperspherical Harmonics *ab-initio* method for the ^{4}He monopole form factor and the $^3\mathrm{He}(\vec{n}, p)^3\mathrm{H}$ parity-conserving asymmetry. Both these observables have turned out to be very sensitive to the $A = 4$ structure, and therefore to the nuclear interaction. In particular, our predictions for the ^{4}He monopole form factor are in good agreement with the experimental data and with the theoretical predictions of Refs. [25–27], but not with those of Ref. [28].

In the future, on the lines presented here, we expect to apply Bayesian analysis for the chiral order truncation error to other processes, especially those of astrophysical interest, as the proton-proton fusion, or the proton-deuteron radiative captures. In the first case, it will be highly appreciated for stellar evolution models, in the second one, it will make the comparison with the available experimental data more meaningful, in order to understand whether a discrepancy between theory and experiment is significant or not. Finally, regarding the ^{4}He monopole form factor, the first issue to be solved will be to understand why theoretical predictions of different groups lead to different results. Therefore, a benchmark calculation is highly desirable. Work along this line is currently underway.

Acknowledgments

The work of A.G. is supported by the U.S. Department of Energy through the Nuclear Theory for New Physics Topical Collaboration, under contract DE-SC0023663. A.G. acknowledges also the support of Jefferson Lab supported by the U.S. Department of Energy under contract DE-AC05-06OR23177.

References

[1] R. Machleidt and F. Sammarruca, Prog. Part. Nucl. Phys. **137**, 104117 (2024)

[2] D.R. Entem and R. Machleidt, Phys. Rev. C **68**, 041001 (2003)

[3] R. Machleidt and D.R. Entem, Phys. Rep. **503**, 1 (2011)

[4] D.R. Entem, R. Machleidt, Y. Nosyk, Phys. Rev. C **96**, 024004 (2017)

[5] M. Piarulli *et al.*, Phys. Rev. C **91**, 024003 (2015)

[6] M. Piarulli *et al.*, Phys. Re. C **94**, 054007 (2016)

[7] A. Baroni *et al.*, Phys. Rev. C **98**, 044003 (2018)

[8] L.E. Marcucci *et al.* Phys. Rev. Lett. **108**, 052502 (2012) [Erratum: **121**, 049901 (2018)]

[9] A. Gnech, L.E. Marcucci, M. Viviani, Phys. Rev. C **109**, 035502 (2024)

[10] A. Baroni *et al.*, Phys. Rev. C **93**, 015501 (2016)

[11] M. Piarulli *et al.*, Phys. Rev. C **87**, 014006 (2013)

[12] A. Kievsky *et al.*, J. Phys. G: Nucl. Part. Phys. **35**, 063101 (2008)

[13] L.E. Marcucci *et al.*, Front. in Phys. **8**, 69 (2020)

[14] A. Gnech, M. Viviani, L.E. Marcucci, Phys. Rev. C **102**, 014001 (2020)

[15] A. Gnech *et al.*, Phys. Rev. C **104**, 035501 (2021)

[16] M. Viviani *et al.*, Few-Body Syst. **65**, 74 (2024)

[17] M. Viviani *et al.*, Phys. Rev. C **102**, 034007 (2020)

[18] M. Viviani *et al.*, Phys. Rev. C **110**, L061001 (2024)

[19] R.J. Hill *et al.*, Rep. Prog. Phys. **81**, 096301 (2018)

[20] J.A. Melendez *et al.*, Phys. Rev. C **100**, 044001 (2019)

[21] Th. Walcher, Phys. Lett. **B31**, 442 (1970)

[22] R.F. Frosch *et al.*, Nucl. Phys. **A110**, 657 (1968)

[23] G. Kobschall *et al.*, Nucl. Phys. **A405**, 648 (1983)

[24] S. Kegel *et al.*, Phys. Rev. Lett. **130**, 152502 (2023)

[25] E. Hiyama, B.F. Gibson, M. Kamimura, Phys. Rev. C **70**, 031001(R) (2004)

[26] N. Michel, W. Nazarewicz, M. Ploszajczak, Phys. Rev. Lett. **131**, 242502 (2023)

[27] Ulf-G. Meißner *et al.*, Phys. Rev. Lett. **132**, 062501 (2024)

[28] S. Bacca *et al.*, Phys. Rev. Lett. **110**, 042503 (2013)